Renewable Energy 146 (2020) 789–801

Contents lists available at ScienceDirect

Renewable Energy

journal homepage: www.elsevier.com/locate/renene

Using the analog ensemble method as a proxy measurement for wind power predictability

M. Shahriari [a, 1], G. Cervone [b, c, *], L. Clemente-Harding [b, 2], L. Delle Monache [c, d]

[a] John and Willie Leone Family Department of Energy and Mineral Engineering, The Pennsylvania State University, University Park, PA, 16802, USA
[b] Institute for CyberScience and Department of Geography, The Pennsylvania State University, University Park, PA, 16802, USA
[c] National Center for Atmospheric Research, Boulder, CO, USA
[d] Center for Western Weather and Water Extremes, Scripps Institution of Oceanography, University of California San Diego, California

ARTICLE INFO

Article history:
Received 20 July 2018
Received in revised form
13 April 2019
Accepted 21 June 2019
Available online 26 June 2019

Keywords:
Wind power forecasting
Probabilistic forecast
Forecast uncertainty
Analog ensemble
Wind output volatility

ABSTRACT

Wind power forecast uncertainty exposes wind farms to volatile real-time electricity prices and increases wind power integration costs. Wind power forecast uncertainty could address these challenges and facilitate the process of siting suitable wind farm locations. In this study, the Analog Ensemble (AnEn) is employed to generate probabilistic wind speed forecasts at 80-m height using past forecast and analysis fields from the Global Forecast System (GFS). The AnEn predictions are used as proxy measurements for how difficult it is to estimate wind speed at different locations in the contiguous United States. The results show significant spatial variations in the wind speed error over the domain. This measure of uncertainty is paramount when determining the most suitable locations for large wind farms. We observed that locations with higher average wind speed are associated with larger degrees of forecast uncertainty which increases the difficulty to predict wind speed at these locations. Our analysis showed high correlation between forecast uncertainty and wind power output volatility which indicates higher risk of operating in real time electricity markets for wind farms located in areas with higher wind speeds. Further, a simple risk analysis using Sharpe ratio was performed to evaluate the riskiness of wind farms in the U.S.

1. Introduction

Wind power is a renewable source that can provide a sustainable solution to meet the energy demand of a growing economy, and at the same time help mitigate the effects of greenhouse gas emissions associated with traditional fossil fuels. Using wind energy for a portion of the energy supply also increases energy security by decreasing the reliance on traditional fossil fuels. Despite these benefits, relying on wind energy presents challenges due to the intermittency of wind energy and the uncertainty associated with day-ahead forecasts. These challenges primarily arise due to variable energy output which, unlike traditional generators, is correlated to rapidly changing local atmospheric conditions [1–3]. These issues must be addressed to assure system stability, reliability, and power quality [4]. As a result, the power system operators need to incorporate different types of reserve capacity such as ancillary services and capacity markets to reliably satisfy real-time demand [5,6]. However, improved forecasting methods that capture the uncertainty associated with wind forecasts could reduce the required reserve capacity, facilitate the penetration of wind power into electricity grids, and decrease wind balancing costs as it decreases the need for fast ramping of reserve capacity [7–14]. While advanced forecasting could further improve the reliability of real time and day-ahead electricity markets [11,15,16], generation resource mix has significant impact on how improved forecasting capability will influence system operation over different time scales [17]. Further, good forecasting could reduce wind power curtailment [12] and could help wind farm owners with their optimal bidding strategies [15,18].

* Corresponding author. Institute for CyberScience and Department of Geography, The Pennsylvania State University, University Park, PA, 16802, USA.
E-mail addresses: mehdi.shahriari@alumni.psu.edu (M. Shahriari), cervone@psu.edu (G. Cervone), laura.e.harding@erdc.dren.mil (L. Clemente-Harding), ldellemonache@ucsd.edu (L. Delle Monache).
[1] Present address for Mehdi Shahriari: Ascend Analytics, 1877 Broadway #706, Boulder, CO 80302.
[2] Affiliation: Engineer Research and Development Center: Geospatial Research Laboratory, Alexandria, VA 22315, USA.

https://doi.org/10.1016/j.renene.2019.06.132
0960-1481/

1.1. Wind power forecasting

There are various methods that can be used for wind speed and wind power forecasting. Wu and Hong [12] reviewed available methods for wind power forecasting and categorized these methods into four groups: numerical weather prediction (NWP) models, statistical models, Artificial Neural Network (ANN) models and hybrid models. Soman et al. [15] also categorized wind power and wind speed forecasting methods into the four mentioned categories. They argued that NWP models are preferred for long term forecasting (1 day–1 week ahead) while statistical and ANN methods perform better over short-term periods (30-min to 6-h ahead). Multiple other studies have focused on combining different methods to reduce the error of short-term wind power forecasting [11,19–32].

Another way to categorize forecasting methods is based on their methodology and their output; whether they are deterministic or probabilistic. Probabilistic methods have the advantage of quantifying the uncertainty associated with the forecast [10,14,33]. Knowledge of forecast uncertainty is critical to enabling users of forecast model output to make informed decisions encapsulating a range of potential outcomes [34]. Forecast uncertainty could hinder the performance of gas generators and increase the operational costs of the power system [14]. It could also hinder integration of offshore wind power into the grid and increase the required reserve capacity [35,36].

Zhang et al. [33] reviewed current probabilistic methods on wind power forecasting and discussed the advantages and challenges associated with these methods. Ensemble models can be used to generate probabilistic wind speed/power forecasts and to quantify the uncertainty of these forecasts. Many of these ensemble members are created by running a NWP model several times. The degree of the similarity between ensemble members is often used to show the uncertainty of the forecast [10]. However, calculating the forecast uncertainty with ensemble forecast models is computationally intensive. It grows with each forecast lead time, and will always be present due to imperfect initial conditions and numerical approximations required for (NWP) models [37]. The Analog Ensemble (AnEn), on the other hand, is computationally efficient as it does not require a NWP model to be run several times and it does not depend on initial conditions [3,38].

1.2. The Analog Ensemble (AnEn)

The AnEn approach is used to generate probabilistic forecasts of 80-m wind speed using a historical repository of NWP forecasts and corresponding analysis fields. Delle Monache et al. [38] have shown that the AnEn can generate well calibrated probabilistic forecasts. In the traditional Delle Monache et al. [38] implementation, a current deterministic forecast, a set of corresponding historical forecasts and their verifying observations, and a similarity metric are used to select the most similar past forecasts to the current deterministic forecast. In this study, analysis fields are used as the observational dataset, in lieu of in-situ observations. Once similarity is determined, the analysis corresponding to the best matching historical forecasts are used to generate a probabilistic prediction. The definition of the similarity metric is critical to the AnEn technique. The similarity computes the difference between a multi-variate current deterministic forecast and a set of historical forecasts. This action can be thought of as determining a measure of distance. In general, and for the purpose of this study, a forecast is assumed to be a multi-variate time series, where the time dimension is the forecast lead time of the NWP and the number of variables is the physical predicted variables output by the NWP.

Previous studies have successfully generated probabilistic forecasts using AnEn and have shown its superiority over other methods [3,38]. Alessandrini et al. [39] used the AnEn to create probabilistic forecasts of solar power for three solar farms in Italy. Comparison with Quantile Regression (QR) and Persistence Ensemble (PeEn) showed advantages to utilizing the AnEn technique for forecasting rare events. Vanvyve et al. [40] showed that, when combined with long term historical atmospheric data, the AnEn technique is capable of evaluating the suitability of wind farm development in a specific area. They argued that the AnEn provides an accurate estimate of the uncertainty associated with the forecasts and thus “ensure(s) the confidence of investors.” Junk et al. [41] used a novel predictor weighting method to optimize the weights on different parameters over different seasons. Their results indicated that these optimal weights will increase the accuracy of the forecasts.

The proposed methodology uses a two-dimensional grid to estimate the probability distribution of wind speed (the predictand) given the values of predictor variables such as temperature, pressure, geopotential height, U-component, and V-component of the wind. The modified wind power curves and air density values are used to generate probabilistic wind power forecasts. Our results provide a grid of wind power values and the uncertainty associated with each estimate. The uncertainty in estimation is related to other factors such as topography, land cover, and wind resources. This is achieved by using a GIS system to compute the correlation between the uncertainty and geographical characteristics. Further, the NREL Eastern Wind Dataset is used (which includes more than 1300 simulated wind farms) to calculate several performance measures (such as capacity factor and output volatility) for each wind farm. Then, each wind farm is associated with an uncertainty value. Finally, the correlation between the uncertainty index and performance measures are calculated. While previous studies have used standard deviation of wind output as a measure for the risk associated with wind power [42–44], in this research the correlation between uncertainty and output volatility is used to evaluate the suitability of this measure (i.e., standard deviation of output) for determining the risk associated with wind farms.

This study has significant applications for investors in renewable energy sector especially wind farm developers. A lower level of uncertainty facilitates the process of submitting bids into day ahead and real-time electricity markets. Thus, building wind farms in regions with lower levels of uncertainty will reduce the real-time operational risks and create a hedge against volatile real-time prices. Further, the links between wind estimate uncertainty and factors such as topography and wind resources, provide wind farm developers with valuable information regarding wind farm siting. This research extends the fundamental knowledge of the community in understanding the AnEn technique and can address the knowledge related to uncertainty associated with the variability of renewable resources, local atmospheric conditions, and the geographic feasibility of forecasting in and for a region of interest.

Thus, our major contributions to the previous body of research on wind power forecast and wind forecast uncertainty are: 1) Implementation of the AnEn in a bigger scale using 2D grid data, 2) introducing a measure to identify high risk locations for wind farm development, 3) studying the factors that could influence wind forecast uncertainty, and 4) evaluating the appropriateness of standard deviation of output as a measure for riskiness of wind farms.

2. Data

Global Forecast System (GFS) forecasts and analyses are used in this study. The GFS model is maintained by the National Centers for Environmental Prediction (NCEP), and it provides global coverage at approximately 28-km resolution (0.25 by 0.25° grid cells) with numerous physical variables available to users. For each of the datasets described, two years worth of data extending from 15 January 2015 to 14 January 2017 have been used. The GFS forecast data is available in 3-h intervals (ranging from 3-h to 384-h ahead) and the analysis data is available in 6-h intervals. In order to have both the forecast and analysis on the same scale, only 6-h intervals from 6-h to 72-h ahead have been used. This range (6-h to 72-h) corresponds to unit commitment and generation dispatch time frame [10]. This time period is important to wind power generators as it can impact their offers in Day Ahead and Real Time electricity markets. All historical forecasts used in this study are initialized at 00.00 UTC. The historical GFS forecasts are used for finding the best analogs and the GFS analysis field as the ground truth to evaluate the model. Table 1 lists the name of physical variables used in this study. The selection of these variables was based on previous literature [38,41]. The independent variable (i.e., variable to estimate) is wind speed at 80-m height and other variables are used to find the best analogs.

2.1. Partitioning of the data

Studies that focus on estimating a variable divide the data into two partitions: one partition for training the model and one partition for evaluating the model. The basic principles imply using one year for training and one year for testing the model. Here, a different method was used to increase the accuracy by artificially increasing the lengths of training and testing periods. This is called leave one out method where all but one day are used to train the data and all the remaining days are used to test the model. This procedure is repeated for all days in the dataset.

3. Methods

3.1. The Analog Ensemble technique

The AnEn technique builds an ensemble of analogs from deterministic NWP output [38]. Analogs are sought independently at each GFS grid and for each lead time. The best matching historical forecasts for the current prediction are selected as the analogs. The best match is determined by the metric described in Refs. [38,45] as follows:

$$F_t, A_{t'} = \sum_{i=1}^{N_v} \frac{w_i}{\sigma_{fi}} \sqrt{\sum_{j=-\tilde{t}}^{\tilde{t}} \left(F_{i,t+j} - A_{i,t'+j}\right)^2} \quad (1)$$

Where F_t is the forecast for which analogs are being sought at the given time t and A_t is an historical forecast at time t' before F_t. $A_{t'}$ is found within the search space. The process is repeated independently for each grid cell (more than 13,000). N_v and w_i are the number of physical predictor variables used to search for the analogs and their associated weights, respectively. As a circular variable, wind direction is handled using circular statistical measures. σ_{fi} is the standard deviation of the time series of past forecasts of a given variable at the same location, $\tilde{t}$ is an integer equal to half the width of the time window over which the metric is computed, and $F_{i,t+j}$ and $A_{i,t'+j}$ are the values of the current and past forecasts time window for a given variable.

The similarity metric describes the quality of the analog chosen and is based upon the similarity of the current deterministic forecast window to the past forecast time windows available in the dataset. Analogs are ranked from most to least similar and can come from any past date within the training period (also known as the search space). Next, the corresponding observations for each of the m best analogs are selected, where m is the number of ensemble members. Note that the GFS analysis fields are used as the observational repository. Together, the corresponding observations generate the m members of the ensemble prediction for the current forecast lead time. Delle Monache et al. [38] showed that the AnEn has several attractive features including the use of higher resolution forecasts and no need for initial conditions, model perturbation strategies, or post processing requirements. The AnEn is able to capture flow-dependent error characteristics and shows superior skill in predicting rare events when compared to state-of-the-art post processing methods [38,45].

Table 1
Parameters used in the AnEn model.

Variable (unit)	Vertical level
Wind speed (m/s)	10-m, 80-m, and 100-m
Wind direction (°)	10-m, 80-m, and 100-m
Temperature (°C)	Surface, and 80-m
Pressure (pa)	Surface, and 80-m
Geopotential height (mb)	Surface, 500 mb, 850 mb, and 925 mb
Boundary layer height (m)	Surface
Gust (m/s)	Surface

3.2. Persistence ensemble

Persistence methods are generally used as a benchmark to evaluate the results from a forecasting model [10,19,46]. The persistence ensemble (PeEn) for each forecast lead time uses the previous observation values for the same hour. Here, the most recent 10 observation values (analysis field) were used so the PeEn has the same number of members as the AnEn. While PeEn is often referred to as the naive predictor [10], it is capable of producing consistent and reliable results over short-term predictions. In this study, the AnEn results were evaluated by comparing them against the PeEn results.

3.3. Validation metrics

The AnEn method creates a probabilistic forecast of the independent variable (wind speed at 80-m) by selecting the best analogs from the past forecasts. To determine the optimal number of analogs (ensemble members), a brute force approach is used testing an increasing size of ensemble members (m = 5, 10, 15, 20, 25, 30). The correlation between the ensemble mean computed using a different number of members and the observation value for each forecast lead time is computed. The bias of AnEn model is also computed by calculating the difference between the observation and the ensemble mean at each point in time and then averaging over all grid cells. The bias shows whether the forecasts have the tendency to be constantly lower or higher than the observations. A good forecast model should have a bias very close to zero. In addition, the root mean square error (RMSE) of the AnEn is computed by using the following equation:

$$RMSE_{AnEn} = \sqrt{\frac{\sum_{i=1}^{n}(A_i - O_i)^2}{n}} \quad (2)$$

Where A_i and O_i are respectively the ensemble mean and

observation at time *i* for a single forecast lead time and a single grid. The RMSE is computed separately for each forecast lead time and for each gird and then averaged over all forecast lead times and then over all grid cells to find the average RMSE of the AnEn.

3.4. Forecast degree of difficulty

We proceed by quantifying the degree of difficulty to predict 80-m wind power over the contiguous U.S. Wind power is influenced by cubic wind speed:

$$power = \frac{1}{2} .\rho. cp.A.V^3 = k.V^3 \quad (3)$$

where ρ is air density, cp is the turbine power coefficient, A is rotor swept area, and V is wind speed (k is used to simplify the explanations). Therefore, wind speed forecasts errors are expected to increase by the power of three. In other words, a forecast error of 1 m/s is not uniformly realized for different values of wind speed. For example, consider two scenarios: 1) forecast is 7 m/s and observation is 6 m/s, 2) forecast is 3 m/s and observation is 2 m/s. In the first scenario, wind power forecast shortfall will be equal to 127 k ($7^3 - 6^3$), while in the second scenario, the shortfall is equal to 19 k ($3^3 - 2^3$). This simple example illustrates the importance of using an accurate measure to quantify wind power forecast uncertainty.

Wind power can be calculated by having data on wind speed and using a power curve of a specific commercial wind turbine. However, standard wind turbine power curves are based on standard air density of 1.225 kg/m^3 and using a single power curve will reduce the accuracy of the results. Therefore, in order to create an accurate measure of wind power forecast uncertainty, data relative to temperature, pressure and relative humidity were used to calculate air density for each point in our time series.

The following equation was used to perform the computations:

$$\rho = \left(\frac{P_d}{R_d \,.\, T}\right) + \left(\frac{P_v}{R_v \,.\, T}\right) \quad (4)$$

where ρ is air density, P_d and P_v are pressure of dry air and water vapor, R_d and R_v are gas content for dry air and water vapor, and T is the temperature in Kelvin (available from GFS dataset). R_d and R_v are respectively equal to 287.05 and 461.495 $\frac{j}{kg \,.\, degK}$. Vapor pressure is calculated as:

$$P_v = RH \,.\, E_s \quad (5)$$

where RH is relative humidity (available from GFS dataset) and E_s is saturation vapor pressure which is calculated as:

$$E_s = c_0 \,.\, 10^{\frac{c_1 \,.\, T_c}{c_2 + T_c}} \quad (6)$$

T_c is the temperature in degree Celsius, and c_0, c_1 and c_2 are some constants and their values are respectively equal to 6.1078, 7.5 and 237.3. After calculating the vapor pressure, air pressure was computed by subtracting vapor pressure from total pressure:

$$P_d = P - P_v \quad (7)$$

where P is the total air pressure (available from GFS dataset). Next, the turbine power curve (Vesta V90 2 MW turbine) was defined by using the data available at [53] and fitting a parametric logistic function on wind speed and wind power. Previous studies have shown that power curves created by parametric logistic functions have high accuracy [54–56].

Since the curve changes for different values of air density, an air density correction was applied and used to calculate wind power production more accurately. The air density correction simply calculates a normalized (corrected) wind speed based on the new air density. The standard wind turbine power curves are based on the standard air density of 1.225 kg/m^3; therefore, if air density is below or above the standard air density, the following correction should be incorporated:

$$V_{norm} = V_{sd} \,.\, \left(\frac{\rho_{norm}}{\rho_{sd}}\right)^{\frac{1}{3}} \quad (8)$$

where V_{norm} and V_{sd} are respectively the normalized wind speed (wind speed at new air density) and standard wind speed (wind speed at standard air density), and ρ_{norm} and ρ_{sd} are the normalized air density and standard air density. Therefore, after estimating wind speed by using the AnEn method, the above correction is applied to calculate a normalized wind speed (i.e., corrected wind speed based on the actual air density) and then use the wind power curve (Fig. 8) to calculate wind power output. This same method is used to calculate wind power for both the AnEn forecasts and GFS analysis.

The standard deviation of the ensemble members is used to calculate the ensemble spread for each point in time. For example, if the estimated wind power from an AnEn model with 10 members provides the following values in kW: (450, 370, 650, 530, 540, 490, 520, 560, 470, 540) for forecast lead time *f*, the standard deviation of these ensemble members (74 kW) is used as a proxy for the degree of difficulty to predict wind power. This is based on the notion that as a probability distribution becomes wider (higher standard deviation), forecasting becomes more challenging and the forecast accuracy decreases. Therefore, forecast degree of difficulty (FDD) is defined as the standard deviation of ensemble members (ensemble spread). For each grid, the ensemble spread is computed for each point in time. The FDD would be calculated by averaging all these ensemble spreads for each of the grid cells.

4. Results

4.1. Results validation

Fig. 1 shows how bias, correlation and RMSE changes as the number of ensemble member increases. Increasing the number of ensemble members increases both bias and correlation which shows a trade-off between increasing the correlation and decreasing the bias. For the RMSE, however, an inflection point could be observed at 15 ensemble members. Based on RMSE and correlation values, the optimum number of ensembles should be a number between 10 and 20. As the number of ensemble member increases from 10 to 20, the percentage increase in bias is larger than the percentage increase in correlation and the percentage increase in RMSE. Further, increasing the number of ensemble members could impact other measures such as statistical consistency and reliability of the AnEn forecasts. Because of the results from this analysis 10 ensemble members were found to be the best number for this study.

4.1.1. RMSE

Fig. 2 shows the RMSE for GFS and AnEn for all grid cells in the contiguous United States. $RMSE_{GFS}$ has been calculated by using GFS forecast as prediction and GFS analysis as observation. To calculate $RMSE_{AnEn}$, GFS analysis field is used as observation and ensemble

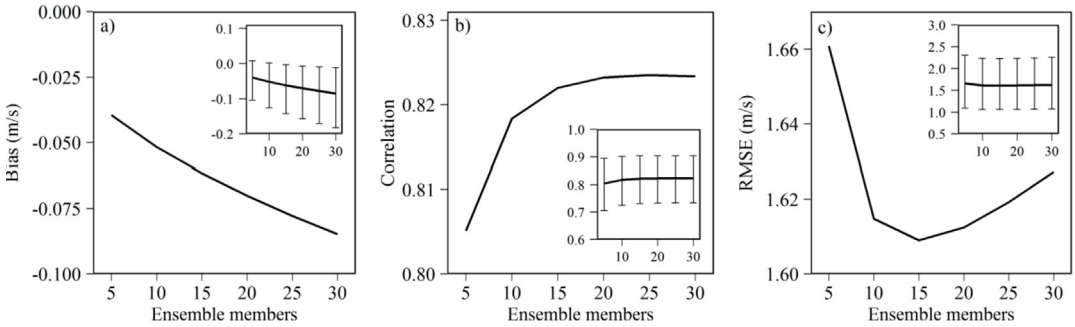

Fig. 1. a) Bias, b) correlation, and c) RMSE for different number of ensemble members. The main plots show the average value over all grid cells while the insets show the average values plus the 5th and 95th percentiles (identified by the error bars).

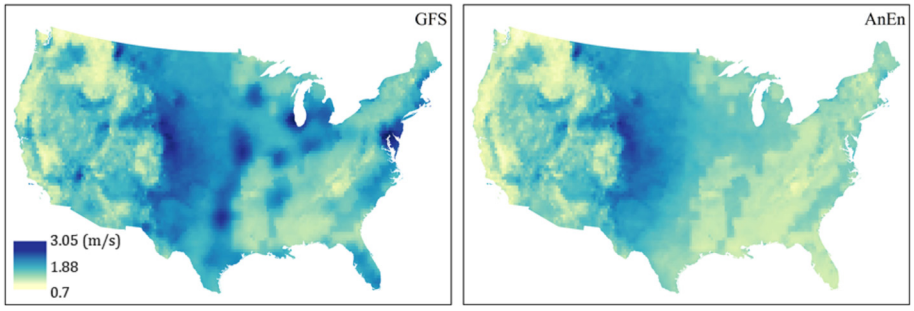

Fig. 2. Root mean square error (RMSE) of AnEn and GFS for all grid cells in the contiguous U.S.

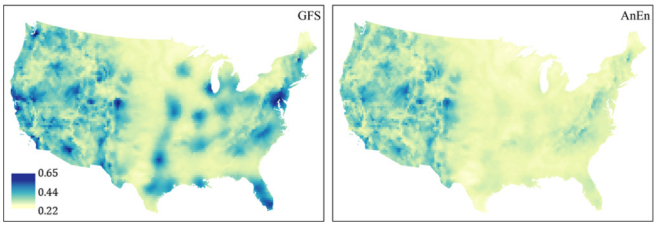

Fig. 3. Normalized root mean square error (nRMSE) of AnEn and GFS for all grid cells in the contiguous U.S.

mean as prediction. For each grid and for each forecast lead time, the ensemble mean was calculated by averaging over all members for each point in time. The RMSE calculates the standard deviation of the errors and illustrate how far the forecasts are from the best fitted line (i.e., how close the forecasts are to the observations). Thus, lower values of RMSE are preferred as they relate to smaller differences between forecasts and observations. The AnEn performs better than GFS especially in locations over the East Coast and the Midwest. In general, locations with higher wind speeds have higher RMSEs. This means that predicting wind speed at these locations would be more difficult and the forecasts are associated with higher degrees of uncertainty. (Refer to Fig. A.11 in Appendix for a U.S. Wind Resource Map.)

Fig. 3 shows the normalized RMSE (nRMSE) for GFS and AnEn methods over the contiguous U.S. The RMSE values are normalized by calculating the ratio of RMSE to mean observation (average wind speed at 80-m) for each point in time. The AnEn performs better than GFS in almost all grid cells especially over the eastern U.S. The nRMSE is useful for evaluating forecast error on a percentage term. This measure calculates forecast error as a percentage of wind speed and provides a tool for evaluating forecast uncertainty by considering the spatial variability of wind resources.

Further the differences between $RMSE_{AnEn}$ and $RMSE_{GFS}$ were calculated and as well as $nRMSE_{AnEn}$ and $nRMSE_{GFS}$ by respectively subtracting $RMSE_{GFS}$ from $RMSE_{AnEn}$ and $nRMSE_{GFS}$ from $nRMSE_{AnEn}$. Fig. 4 shows these differences; the left panel shows the RMSE difference ($RMSE_{AnEn}$ - $RMSE_{GFS}$) and the right panel shows the nRMSE difference ($nRMSE_{AnEn}$ and $nRMSE_{GFS}$). As expected, the maps look identical and show that AnEn is performing better than GFS over all locations. There are few locations where the GFS is doing better than AnEn but the difference is not statistically significant (difference is less than 0.01). The evident difference between East and West U.S. in Fig. 4 is due to the following reasons: 1) Lower wind speed and therefore lower spread in the East, 2) Different weather regiments making it easier to predict the weather in the East, 3) AnEn performance is worse in mountainous areas where prediction is more challenging.

4.1.2. Probabilistic validation methods

Further, several tests were performed to evaluate the statistical consistency, reliability, sharpness, resolution, and value of the AnEn probabilistic forecasts. To perform these tests, two different methods were used. In the first method, 10 grid cells were chosen (from more than 13,000 available over the Contiguous U.S.) based on their $RMSE_{AnEn}$. After calculating the $RMSE_{AnEn}$ for all grid cells, the 10th, 20th, …, 100th percentiles of these RMSEs were computed. By using these percentiles, the data were partitioned into ten groups (smaller than 10th, between 10th and 20th, and so on) and then 1 grid from each group was randomly chosen. Finally, all the tests on these 10 grid cells were performed. In the second method, data from all grid cells were considered and the tests were performed as if they were all from a single grid. Figures for the first

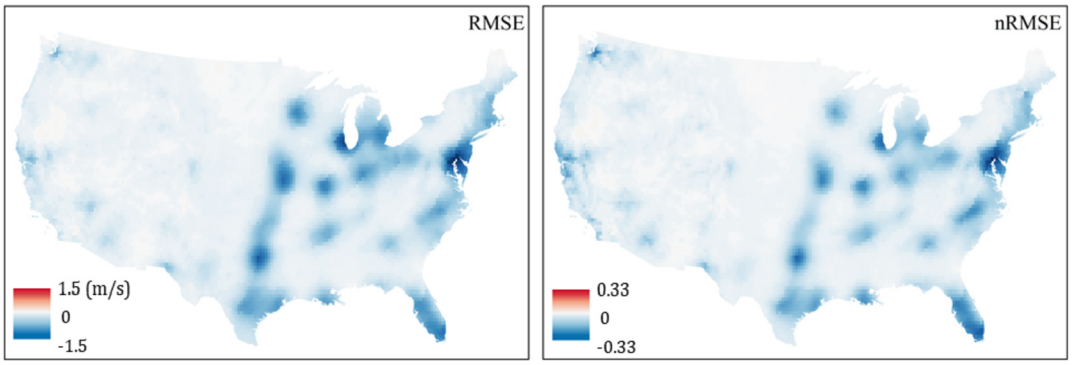

Fig. 4. Left panel shows the RMSE difference ($RMSE_{AnEn}$ - $RMSE_{GFS}$) and the right panel shows the nRMSE difference ($nRMSE_{AnEn}$ - $nRMSE_{GFS}$).

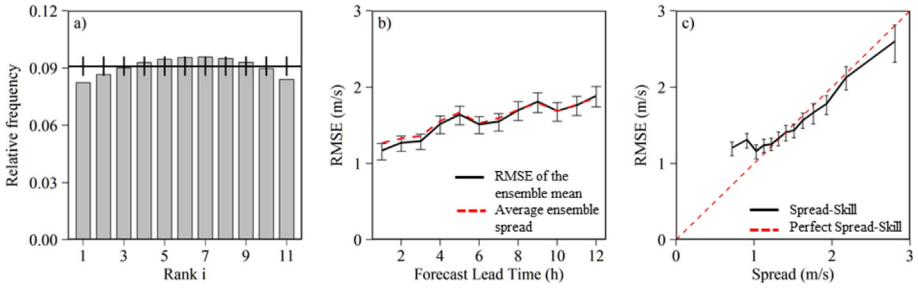

Fig. 5. a) Rank histogram: The black horizontal line shows how a perfectly flat rank histogram should look, b) dispersion diagram: The black line shows the RMSE of the ensemble mean and the dashed red line shows the average ensemble spread. The error bars show the 5th and 95th quantiles for the RMSE, and c) spread-skill: The dashed red line shows the perfect spread-skill relationship. These plots include the results from all grid cells. (For interpretation of the references to colour in this figure legend, the reader is referred to the web version of this article.)

method are included in the Appendix.

First, the statistical consistency of the analog ensembles was measured. Anderson [47] defines a consistent ensemble as an ensemble whose members follow the same distribution as the sample distribution from which the members are chosen. Basically, $n + 1$ bins (n is the number of ensemble members) were chosen and then determined which bin each observation belongs to. If an ensemble is statistically consistent, then an observation could belong to any rank i ($i = 1: n + 1$). In other words, the rank histogram for the ensembles is expected to be flat. This means that the probability of an observation being bigger or smaller than the members should be equal. Panel (a) of Fig. 5 shows the rank histograms for all grid cells in the contiguous U.S. Although the rank histogram is not completely flat and shows a slight tendency towards over dispersion, in general the AnEn has a very promising statistical consistency.

While the rank histograms illustrate the statistical consistency of the model averaged over all forecast lead times, dispersion diagrams are capable of showing the statistical consistency of the model over all forecast lead times. In a dispersion diagram, variability of two parameters are shown over various forecast lead times: RMSE of the ensemble mean and average ensemble variance (ensemble spread). For a statistically consistent ensemble, these two parameters should be very close and highly correlated. Panel (b) of Fig. 5 shows the dispersion diagram for all grid cells. The two measures almost overlap each other which exhibits good statistical consistency of the AnEn.

Another useful measure for determining the statistical consistency of an ensemble model is the spread-skill diagram. This diagram is created by binning the ensemble spread (in this work, specifically, using 10 bins) and plotting it against root mean square error (RMSE) of the ensemble. The advantage here is that RMSE is not being computed against average spread, but rather compared at all values of the ensemble spread [38,48,49]. Thus, for an ensemble to be statistically consistent, ensemble RMSE and ensemble spread must be equal for all values of the ensemble spread. Panel (c) of Fig. 5 shows the spread-skill diagrams for all grid cells. Ensemble RMSE and ensemble spread are very close for almost all values of the ensemble spread. This exhibits the statistical consistency of our AnEn method.

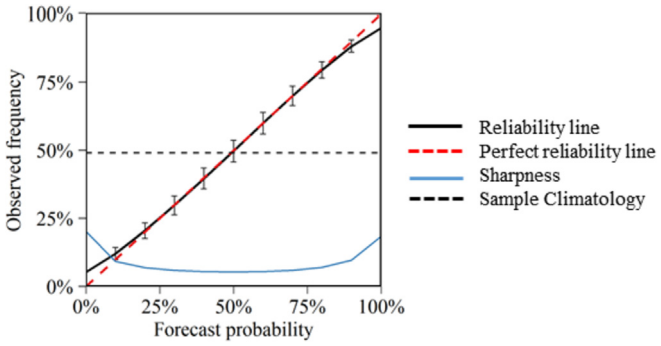

Fig. 6. Reliability diagrams for all grid cells. The black line with error bars shows the reliability line and the blue line shows the sharpness. The black dashed line is sample climatology (observed frequency of wind speed greater than 5 m/s) and the red dashed line is the perfect reliability line. (For interpretation of the references to colour in this figure legend, the reader is referred to the web version of this article.)

Further, the reliability of the ensemble results is tested by using

the reliability diagram. An ensemble is reliable if the forecasted probability of observing an event is equal to the actual observed frequency. A reliability diagram evaluates this condition by plotting the forecast probability against the observed relative frequency [38]. This is achieved by binning the observed occurrences and calculating the observed relative frequency for each bin by dividing the number of observed occurrences by the number of forecasts [50]. Thus, a completely reliable model should follow a 1:1 diagonal line [38,51]. Another important measure to verify an ensemble is the sharpness of the model. If a model produces forecast values closer to the edges (0% or 100%) then it is said that the model is sharper. This measure is important as "a sharper forecast leads to better resolution" [38]. Fig. 6 shows the reliability and sharpness diagrams for all grid cells. The observed frequency and the forecast probability match closely which shows the reliability of the AnEn model. Further, the AnEn sharpness is evident as the highest values are observed along the extreme probabilities (0% or 100%).

The Brier skill score (BSS) is often used to evaluate the accuracy of a probabilistic forecast [52]. This measure is decomposed into three elements: reliability, resolution, and uncertainty [38,39]. The uncertainty does not depend on the model and is only influenced by the sample climatology. The resolution shows the model ability to forecast whether an event occurs or not. The reliability measures the similarity between the forecasted probabilities and the true probabilities. A good probabilistic model should have high resolution and low reliability (best value is 0). The reliability and resolution of the AnEn model is compared with the reliability and resolution of the PeEn model. Panel (a) of Fig. 7 shows the BSS for AnEn and PeEn. Panel (b) of Fig. 7 shows the reliability of the AnEn and PeEn models. The reliability values for AnEn is much smaller than PeEn which shows its superiority over PeEn. Panel (c) of Fig. 7 shows that the AnEn has a much higher resolution than the PeEn model.

Finally, the continuous ranked probability score (CRPS) of the AnEn and PeEn models was calculated. CRPS uses the full probabilistic distribution (where reliability diagrams and BSS use values above a threshold, i.e., wind speeds above 5 m/s) to compare several ensemble systems [39]. Lower CRPS scores are preferred as they illustrate that the cumulative distribution function (CDF) of the probabilistic forecasts are very similar to the CDF of the observations. Panel (d) of Fig. 7 also shows the CRPS plots for the AnEn and PeEn models. The AnEn model has lower CRPS values which shows it superiority over PeEn in creating probabilistic distributions of the forecasts.

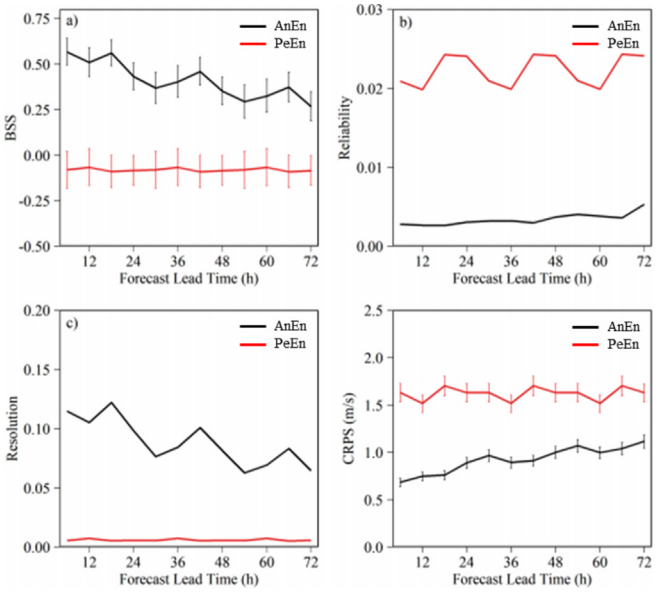

Fig. 7. a) BSS, b) reliability, and c) resolution for AnEn (black) and PeEn (red) for all grid cells in the contiguous U.S. (For interpretation of the references to colour in this figure legend, the reader is referred to the web version of this article.)

4.2. Results discussion

Based on the discussion in section 3.4., ensemble spread and normalized spread are used to show the degree of difficulty to predict wind speed. Fig. 8 shows the ensemble spread and normalized ensemble spread for wind power estimates for all grid cells in the contiguous U.S. The highest values of the ensemble spread are observed along the Midwest which could be related to higher average wind speed in these areas. A normalized ensemble spread measure was computed where the ensemble spread was divided by the average wind power for each point in our time series.

This work also discusses the measure that should be used to assess the degree of difficulty to predict wind power at different locations. While, it can be argued that providing a fair comparison between different locations requires normalizing the difficulty measure based on average wind power estimates, in a real-world situation it might not differ how large the forecast error is relative to the estimated value. In some electricity markets, for example MISO (Midcontinent Independent System Operator) and CAISO (California Independent System Operator),[3] the deviation from the submitted offer results in stiff penalties for the wind generators. Therefore, submitting an offer to the day ahead auction requires accurate estimate of hourly wind generation output for the next day. The system operators do not differentiate offers based on their average wind speed or average wind output. Indeed, the penalties are determined solely based on absolute deviation from the submitted offer in terms of MW. Therefore, in markets like MISO and CAISO, the degree of difficulty would be most appropriately expressed by the ensemble spread. Though, in some markets like PJM,[4] there is no penalty for deviation from the submitted sell offer, building wind farms in regions with higher predictability will decrease system costs of integrating renewables into the grid.

To further investigate why FDD is higher in some regions, the correlation was computed between the ensemble spread and wind power class, elevation and land cover. Data for wind power class is based on wind power classes from NREL [57]. Elevation data was obtained from Ref. [58] and land cover data was obtained from Ref. [59]. Fig. 9 shows the maps for these four variables. Table 2 shows the correlation of ensemble spread with wind power class, elevation and land cover. The results indicate that the highest correlation is between ensemble spread and wind speed which exhibit the difficulty of estimating wind power at locations with higher average wind speed. The correlation between the ensemble spread and elevation is very small which suggests that estimating wind power at higher elevations is not more difficult than estimating wind power at lower elevations.

Further, the relationship was studied in depth between wind farm performance measures such as capacity factor, firm power and volatility. Firm power is defined as the amount of power (i.e., capacity) that is available 79 to 92% of time [60,61]. Volatility is the

[3] Entities that oversee power market operations in their respective region and monitor grid reliability.

[4] Regional Transmission Organization that oversees power market operations in Northeast U.S.

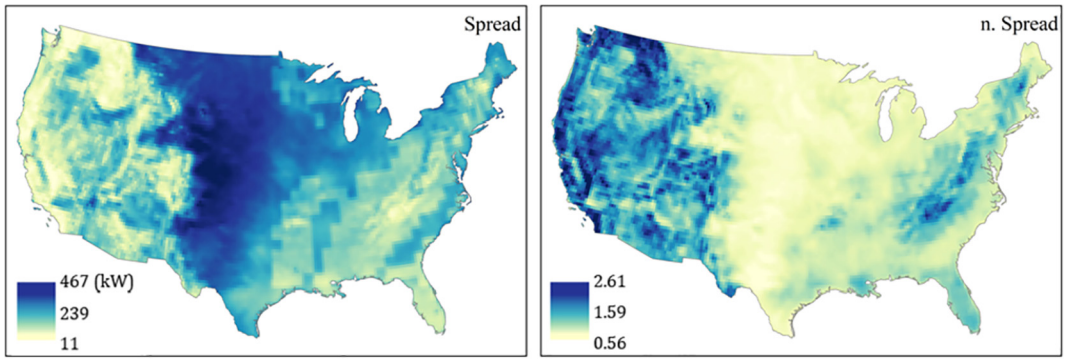

Fig. 8. Wind power ensemble spread and normalized ensemble spread for all grid cells in the contiguous U.S.

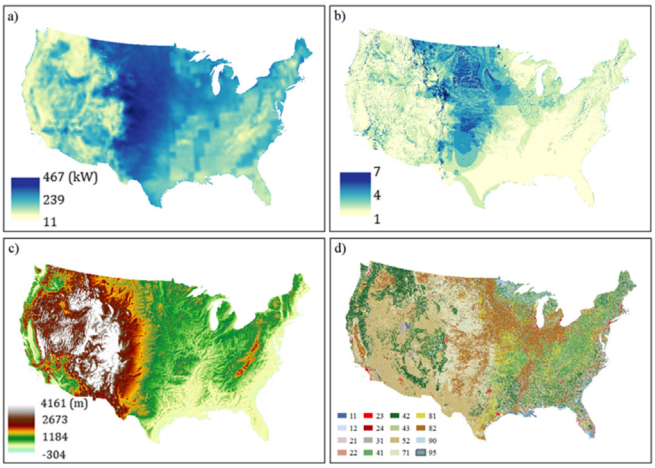

Fig. 9. Maps for a) ensemble spread, b) wind power class, c) elevation, and d) land cover. Refer to Ref. [59] for more details on land cover legend.

Table 2
Ensemble spread correlation with wind power class, elevation, and land cover.

Variable	Wind Power Class	Elevation	Land Cover
Correlation	0.58	−0.12	0.32

Table 3
Ensemble spread correlation with wind sites capacity factor, volatility, and firm power.

Variable	Capacity Factor	Volatility	Firm Power 79%
Correlation	0.96	0.95	0.8

standard deviation of wind power output. For this analysis, the analysis field from GFS is used to calculate the standard deviation, firm power, and capacity factor for each grid in the contiguous U.S. The assumption here is that each grid (i.e., each GFS grid) is an individual wind farm with a single 2 MW wind turbine. Table 3 shows the correlation between the wind power ensemble spread, and wind sites performance measures. The results indicate that wind power ensemble spread is relatively highly correlated with capacity factor, standard deviation and firm power. This basically shows that locations with higher wind power potential (i.e., higher average wind speeds) are more vulnerable to forecast uncertainty. High correlation between wind power ensemble spread and volatility exhibit that higher standard deviation of power will result in higher forecast uncertainty. In other words, volatility is a good indicator of how risky a wind site would be in terms of forecast uncertainty.

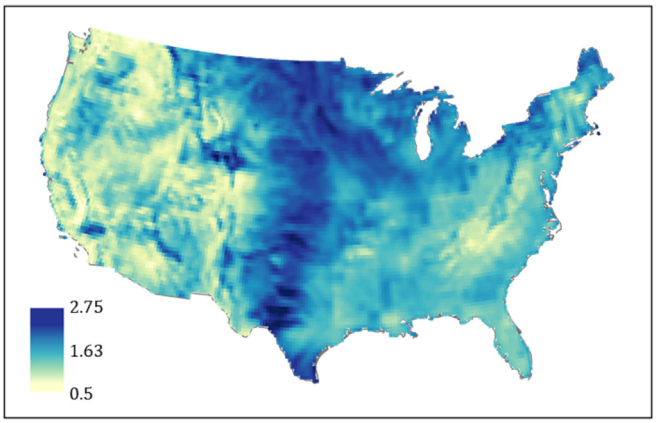

Fig. 10. Sharpe ratio for hypothetical wind farms in contiguous U.S.

Finally, the riskiness of these hypothetical wind farms was evaluated by using the Sharpe ratio. In finance, Sharpe ratio is defined as the ratio of return to risk. In energy studies, the average wind power and standard deviation of wind power are used as proxies for return and risk [42,62]. Here, return is quantified by average wind power and risk is measured by the ensemble spread. Fig. 10 shows the Sharpe ratio for all hypothetical wind farms in the contiguous U.S. Locations along the Midwest (i.e., those with higher average wind speed and higher uncertainty) have higher Sharpe ratios. This means that while these locations have higher forecast uncertainty, they provide higher return per unit of risk. The higher Sharpe ratio implies that the higher return (i.e., average wind power output) of wind sites in this region justifies the higher levels of risk associated with these wind sites. In general, our results indicate a trade-off between return/risk ratio and forecast uncertainty. Wind farms located in the Midwest will provide higher revenues (as a result of larger wind generation) but they also present challenges in terms of forecast uncertainty. This could increase real-time operational risks as wind farms would be more vulnerable to volatile real time prices.

5. Conclusion

We have used the AnEn approach to measure the uncertainty of

wind power estimates and to quantitatively understand how the difficulty to estimate wind power varies over different locations in the contiguous U.S. Our results indicate that ensemble spread is an appropriate proxy for forecast degree of difficulty. This means that we can use the ensemble spread to calculate the uncertainty associated with wind power forecast in different locations and determine the locations where forecasting wind speed is more challenging. It was observed that locations with higher average wind speed are associated with higher forecast uncertainty. This means that wind power forecasting in these areas is more challenging and wind sites are exposed to volatile real time electricity prices. Building wind sites in these regions presents trade-offs in terms of higher return and higher risk.

While previous studies frequently use standard deviation of output to measure how risky a wind site is in terms of output volatility [42,62], the suitability of this measure as a proxy for the degree of difficulty to estimate wind power has not been evaluated. Our results illustrated high correlation between output volatility and forecast uncertainty. This basically means that locations with higher output volatility are associated with higher forecast uncertainty. Further, it was found that ensemble spread is highly correlated with capacity factor and firm power. Finally, the Sharpe ratio showed that locations in Midwestern states (i.e., locations with higher average wind speed) provide higher return per unit of risk.

This work has major policy implications for wind site investors. First, output volatility is shown to be a perfect indicator of the degree of difficulty to estimate wind power. Degree of difficulty (i.e., forecast uncertainty) could only be measured by a probabilistic method. Output volatility, on the other hand, can be evaluated using a deterministic forecast and hence loosen the requirements for more complicated probabilistic forecasts. Further, in general locations with higher average wind speed provide higher return per unit of risk. This means that higher average production in these areas could justify the higher volatility and forecast uncertainty of the wind sites in these regions. Despite this potentially profitable result, however, risk averse investors could still choose locations with smaller volatility and forecast uncertainty to reduce real time operational risks.

Acknowledgement

The Authors are thankful to Seth Blumsack (Penn State) and Elena Sava (Penn State) for their comments and suggestions which helped to greatly improve this paper. Work performed under this project has been partially funded by the National Science Foundation (NSF) award, #1639707.

Appendix A

Appendix A.1. U.S. Wind Speed Map

Figure A.11 shows U.S. annual average wind speed calculated 80-m height. Wind speed estimates have been calculated by AWS Truepower and the map has been created by NREL.

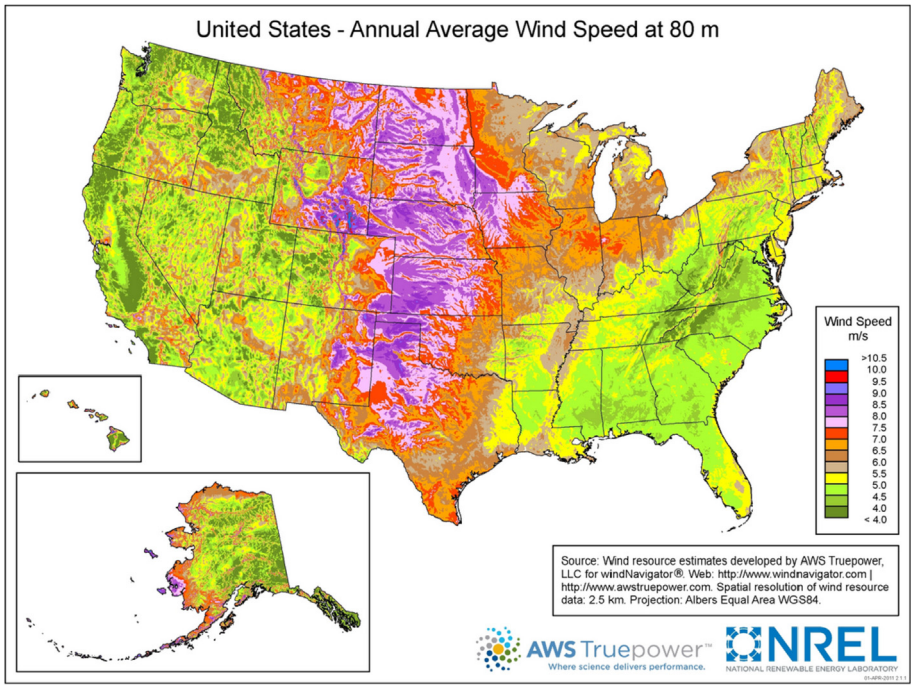

Fig. A.11. Annual average wind speed in US. (Wind resource estimates are developed by AWS Truepower and the map has been created by NREL. Source: https://www.nrel.gov/gis/images/80m_wind/USwind300dpe4-11.jpg)

Appendix A.2. Rank Histograms

Figure A.12 shows the rank histograms for the selected 10 grid cells. $RMSE_{AnEn}$ increases as we move from left to right and top to bottom. In other words, the top left grid has an $RMSE_{AnEn}$ in the first decile and the bottom right grid has an $RMSE_{AnEn}$ in the last decile.

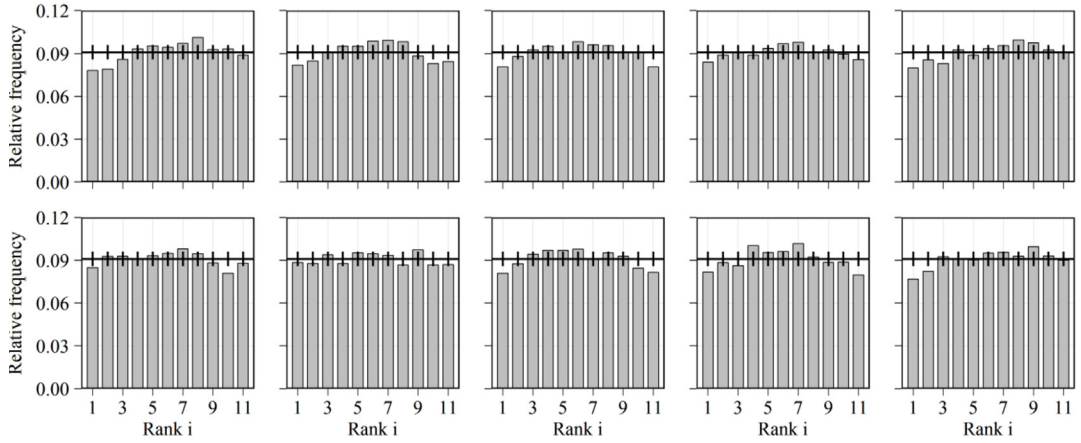

Fig. A.12. Rank histograms for the 10 selected grids. RMSE increases as move from left to right and top to bottom.

Appendix A.2. Dispersion Diagrams

Figure A.13 shows the dispersion diagrams for the selected 10 grid cells. In all grid cells, the two measures almost overlap each other which exhibits good statistical consistency of the AnEn.

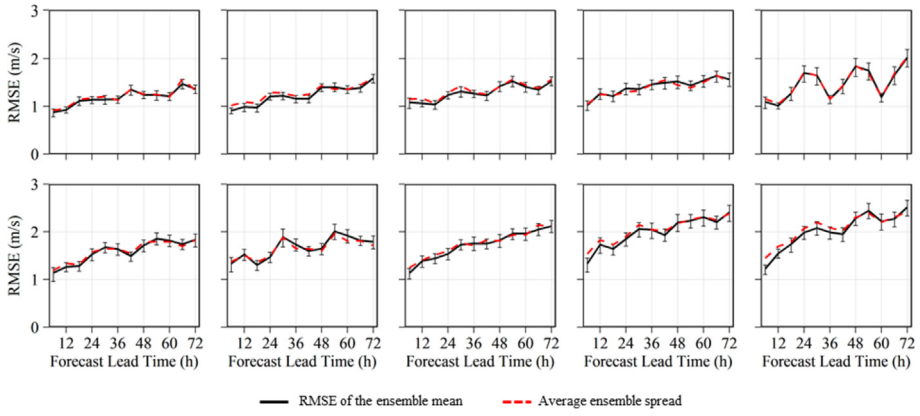

Fig. A.13. Dispersion diagrams for the 10 selected grids. The black line shows the RMSE of the ensemble mean and the dashed red line shows the average ensemble spread. The error bars show the 5th and 95th quantiles for the RMSE.

Appendix A.3. Spread Skill Diagrams

Figure A.14 shows the spread-skill diagrams for the 10 selected grid cells.

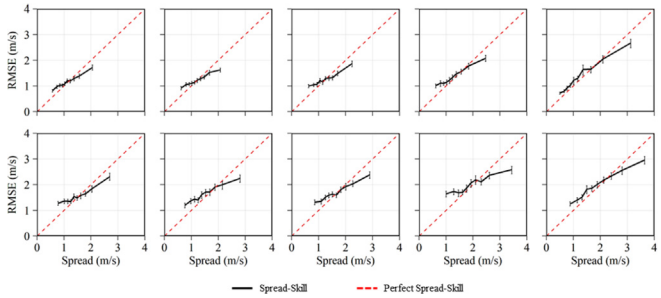

Fig. A.14. Spread-skill plot for the 10 selected grids. The dashed red line shows the perfect spread-skill relationship.

Appendix A.4. Reliability Diagrams

Figure A.15 shows the reliability and sharpness diagrams for the selected 10 grid cells. Over all grid cells, the observed frequency and the forecast probability match closely. Further, the AnEn sharpness is illustrated by high values along the extreme probabilities (0% or 100%).

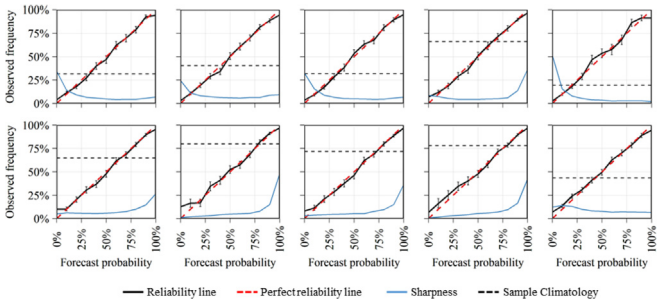

Fig. A.15. Reliability diagrams for the selected 10 grids. The black line with error bars shows the reliability line and the blue line shows the sharpness. The black dashed line is sample climatology (observed frequency of wind speed greater than 5 m/s) and the red dashed line is the perfect reliability line.

Appendix A.5. BSS

Figures A.16, A.17, A.18 show the BSS, reliability and resolution plots for the selected 10 grid cells. These plots show that AnEn performs much better than PeEn.

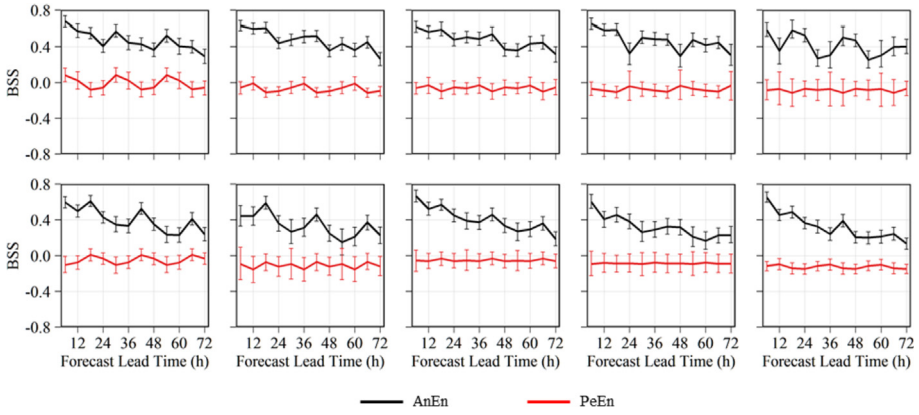

Fig. A.16. Briar skill score (BSS) of AnEn (black lines) and PeEn (red lines) for the selected 10 grids.

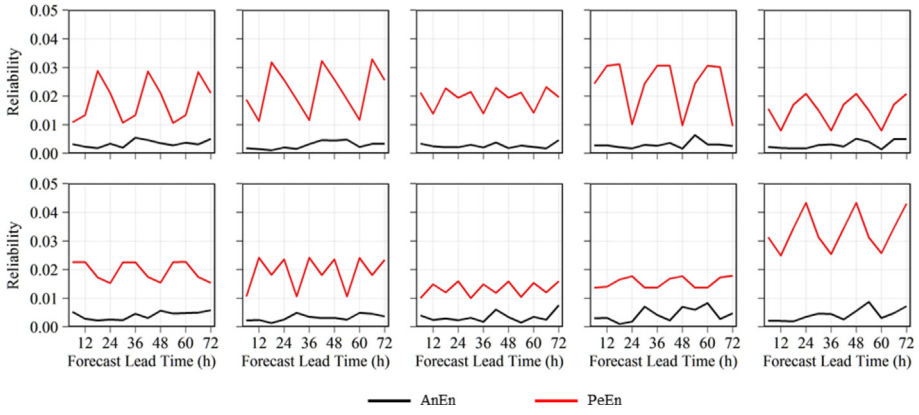

Fig. A.17. Reliability of AnEn (black lines) and PeEn (red lines) for the selected 10 grids.

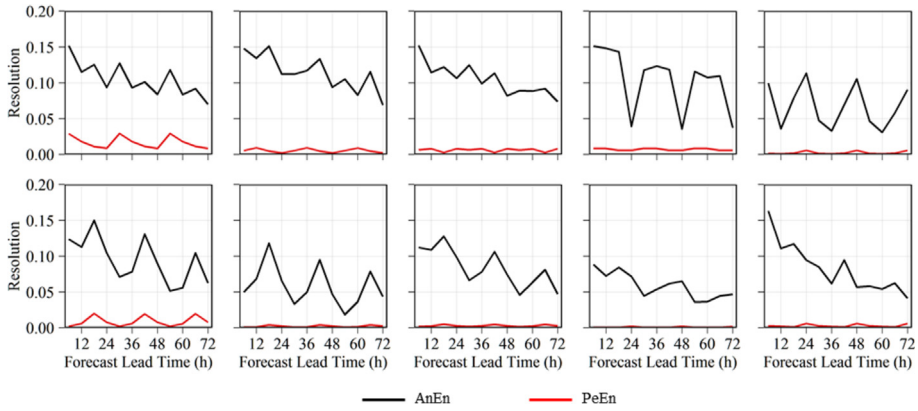

Fig. A.18. Resolution of AnEn (black lines) and PeEn (red lines) for the selected 10 grids.

Appendix A.6. CRPS

Figure A.19 shows the CRPS for the selected 10 grids. AnEn has a lower CRPS compared to the PeEn.

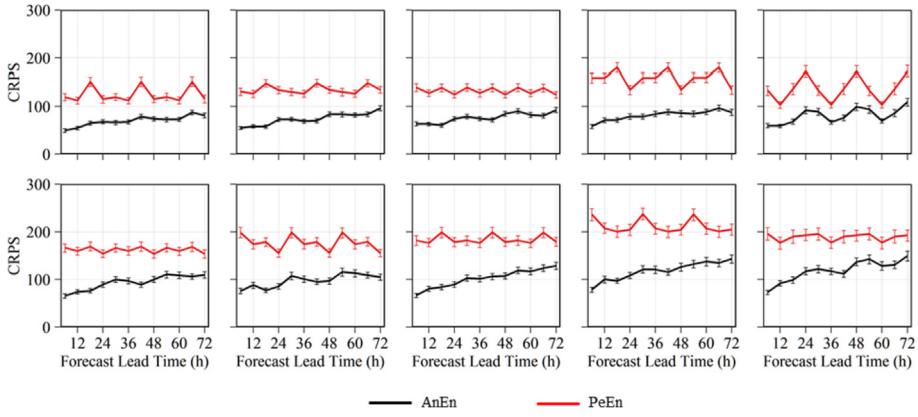

Fig. A.19. Continuous ranked probability score (CRPS) of the AnEn and PeEn models for the selected 10 grids.

References

[1] J.P. Lopes, N. Hatziargyriou, J. Mutale, P. Djapic, N. Jenkins, Integrating distributed generation into electric power systems: a review of drivers, challenges and opportunities, Electr. Power Syst. Res. 77 (9) (2007) 1189–1203.

[2] G. Boyle, Renewable Electricity and the Grid: the Challenge of Variability, Earthscan, 2012.

[3] S. Alessandrini, L. Delle Monache, S. Sperati, J. Nissen, A novel application of an analog ensemble for short-term wind power forecasting, Renew. Energy 76 (2015) 768–781.

[4] S. Vazquez, S.M. Lukic, E. Galvan, L.G. Franquelo, J.M. Carrasco, Energy storage systems for transport and grid applications, IEEE Trans. Ind. Electron. 57 (12) (2010) 3881–3895.

[5] L. Hirth, The market value of variable renewables: the effect of solar wind power variability on their relative price, Energy Econ. 38 (2013) 218–236.

[6] C.-K. Woo, I. Horowitz, J. Moore, A. Pacheco, The impact of wind generation on the electricity spot-market price level and variance: the Texas experience, Energy Policy 39 (7) (2011) 3939–3944.

[7] A. Botterud, J. Wang, C. Monteiro, V. Miranda, Wind power forecasting and electricity market operations, in: Proc. of the IAEE Int. Conf, 2009.

[8] M. Lei, L. Shiyan, J. Chuanwen, L. Hongling, Z. Yan, A review on the forecasting of wind speed and generated power, Renew. Sustain. Energy Rev. 13 (4) (2009) 915–920.

[9] X. Wang, P. Guo, X. Huang, A review of wind power forecasting models, Energy Procedia 12 (2011) 770–778.

[10] A.M. Foley, P.G. Leahy, A. Marvuglia, E.J. McKeogh, Current methods and advances in forecasting of wind power generation, Renew. Energy 37 (1) (2012) 1–8.

[11] W.P. Mahoney, K. Parks, G. Wiener, Y. Liu, W.L. Myers, J. Sun, L. Delle Monache, T. Hopson, D. Johnson, S.E. Haupt, A wind power forecasting system to optimize grid integration, IEEE Trans. Sustain. Energy 3 (4) (2012) 670–682.

[12] Y.-K. Wu, J.-S. Hong, A literature review of wind forecasting technology in the world, in: Power Tech, 2007 IEEE Lausanne, IEEE, 2007, pp. 504–509.

[13] M. Marquis, J. Wilczak, M. Ahlstrom, J. Sharp, A. Stern, J.C. Smith, S. Calvert, Forecasting the wind to reach significant penetration levels of wind energy, Bull. Am. Meteorol. Soc. 92 (9) (2011) 1159–1171.

[14] E. Xydas, M. Qadrdan, C. Marmaras, L. Cipcigan, N. Jenkins, H. Ameli, Probabilistic wind power forecasting and its application in the scheduling of gas-fired generators, Appl. Energy 192 (2017) 382–394.

[15] S.S. Soman, H. Zareipour, O. Malik, P. Mandal, A review of wind power and wind speed forecasting methods with different time horizons, in: North American Power Symposium (NAPS), 2010, IEEE, 2010, pp. 1–8.

[16] A. Botterud, Z. Zhou, J. Wang, J. Sumaili, H. Keko, J. Mendes, R.J. Bessa, V. Miranda, Demand dispatch and probabilistic wind power forecasting in unit commitment and economic dispatch: a case study of Illinois, IEEE Trans. Sustain. Energy 4 (1) (2013) 250–261.

[17] Q. Wang, H. Wu, A.R. Florita, C.B. Martinez-Anido, B.-M. Hodge, The value of improved wind power forecasting: grid flexibility quantification, ramp capability analysis, and impacts of electricity market operation timescales, Appl. Energy 184 (2016) 696–713.

[18] G. Ferruzzi, G. Cervone, L. Delle Monache, G. Graditi, F. Jacobone, Optimal bidding in a day-ahead energy market for micro grid under uncertainty in renewable energy production, Energy 106 (2016) 194–202.

[19] C.W. Potter, M. Negnevitsky, Very short-term wind forecasting for tasmanian power generation, IEEE Trans. Power Syst. 21 (2) (2006) 965–972.

[20] Y. Che, X. Peng, L. Delle Monache, T. Kawaguchi, F. Xiao, A wind power forecasting system based on the weather research and forecasting model and

kalman filtering over a wind-farm in Japan, J. Renew. Sustain. Energy 8 (1) (2016), 013302.
[21] J. Liu, X. Wang, Y. Lu, A novel hybrid methodology for short-term wind power forecasting based on adaptive neuro-fuzzy inference system, Renew. Energy 103 (2017) 620–629.
[22] Y. Zhao, L. Ye, Z. Li, X. Song, Y. Lang, J. Su, A novel bidirectional mechanism based on time series model for wind power forecasting, Appl. Energy 177 (2016) 793–803.
[23] C. Wan, Z. Xu, P. Pinson, Z.Y. Dong, K.P. Wong, Probabilistic forecasting of wind power generation using extreme learning machine, IEEE Trans. Power Syst. 29 (3) (2014) 1033–1044.
[24] H.-z. Wang, G.-q. Li, G.-b. Wang, J.-c. Peng, H. Jiang, Y.-t. Liu, Deep learning based ensemble approach for probabilistic wind power forecasting, Appl. Energy 188 (2017) 56–70.
[25] G. Osorio, J. Matias, J. Catalao, Short-term wind power forecasting using adaptive neuro-fuzzy inference system combined with evolutionary particle swarm optimization, wavelet transform and mutual information, Renew. Energy 75 (2015) 301–307.
[26] H. Quan, D. Srinivasan, A. Khosravi, Short-term load and wind power forecasting using neural network-based prediction intervals, IEEE Trans. Neural Netw. Learn. Syst. 25 (2) (2014) 303–315.
[27] J. Shi, Z. Ding, W.-J. Lee, Y. Yang, Y. Liu, M. Zhang, Hybrid forecasting model for very-short term wind power forecasting based on grey relational analysis and wind speed distribution features, IEEE Trans. Smart Grid 5 (1) (2014) 521–526.
[28] A. Kavousi-Fard, A. Khosravi, S. Nahavandi, A new fuzzy-based combined prediction interval for wind power forecasting, IEEE Trans. Power Syst. 31 (1) (2016) 18–26.
[29] S. Li, P. Wang, L. Goel, Wind power forecasting using neural network ensembles with feature selection, IEEE Trans. Sustain. Energy 6 (4) (2015) 1447–1456.
[30] S. Fang, H.-D. Chiang, A high-accuracy wind power forecasting model, IEEE Trans. Power Syst. 32 (2) (2017) 1589–1590.
[31] C. Wan, J. Lin, J. Wang, Y. Song, Z.Y. Dong, Direct quantile regression for nonparametric probabilistic forecasting of wind power generation, IEEE Trans. Power Syst. 32 (4) (2017) 2767–2778.
[32] L. Cavalcante, R.J. Bessa, M. Reis, J. Browell, Lasso vector autoregression structures for very short-term wind power forecasting, Wind Energy 20 (4) (2017) 657–675.
[33] Y. Zhang, J. Wang, X. Wang, Review on probabilistic forecasting of wind power generation, Renew. Sustain. Energy Rev. 32 (2014) 255–270.
[34] P.A. Hirschberg, E. Abrams, A. Bleistein, W. Bua, L.D. Monache, T.W. Dulong, J.E. Gaynor, B. Glahn, T.M. Hamill, J.A. Hansen, et al., A weather and climate enterprise strategic implementation plan for generating and communicating forecast uncertainty information, Bull. Am. Meteorol. Soc. 92 (12) (2011) 1651–1666.
[35] C. Archer, H. Simao, W. Kempton, W. Powell, M. Dvorak, The challenge of integrating offshore wind power in the us electric grid. part i: wind forecast error, Renew. Energy 103 (2017) 346–360.
[36] H. Simao, W. Powell, C. Archer, W. Kempton, The challenge of integrating offshore wind power in the us electric grid. part ii: simulation of electricity market operations, Renew. Energy 103 (2017) 418–431.
[37] E.N. Lorenz, Deterministic nonperiodic flow, J. Atmos. Sci. 20 (2) (1963) 130–141.
[38] L. Delle Monache, F.A. Eckel, D.L. Rife, B. Nagarajan, K. Searight, Probabilistic weather prediction with an analog ensemble, Mon. Weather Rev. 141 (10) (2013) 3498–3516.
[39] S. Alessandrini, L. Delle Monache, S. Sperati, G. Cervone, An analog ensemble for short-term probabilistic solar power forecast, Appl. Energy 157 (2015) 95–110.
[40] E. Vanvyve, L. Delle Monache, A.J. Monaghan, J.O. Pinto, Wind resource estimates with an analog ensemble approach, Renew. Energy 74 (2015) 761–773.
[41] C. Junk, L. Delle Monache, S. Alessandrini, G. Cervone, L. von Bremen, Predictor-weighting strategies for probabilistic wind power forecasting with an analog ensemble, Meteorol. Z. 24 (4) (2015) 361–379.
[42] B. Drake, K. Hubacek, What to expect from a greater geographic dispersion of wind farms? a risk portfolio approach, Energy Policy 35 (8) (2007) 3999–4008.
[43] N.S. Thomaidis, F.J. Santos-Alamillos, D. Pozo-Vazquez, J. Usaola-Garcıa, Optimal management of wind and solar energy resources, Comput. Oper. Res. 66 (2016) 284–291.
[44] D.P. Neto, E.G. Domingues, A.P. Coimbra, A.T. de Almeida, A.J. Alves, W.P. Calixto, Portfolio optimization of renewable energy assets: hydro, wind, and photovoltaic energy in the regulated market in Brazil, Energy Econ. 64 (2017) 238–250.
[45] L. Delle Monache, T. Nipen, Y. Liu, G. Roux, R. Stull, Kalman filter and analog schemes to postprocess numerical weather predictions, Mon. Weather Rev. 139 (11) (2011) 3554–3570.
[46] X. Zhao, S. Wang, T. Li, Review of evaluation criteria and main methods of wind power forecasting, Energy Procedia 12 (2011) 761–769.
[47] J.L. Anderson, A method for producing and evaluating probabilistic forecasts from ensemble model integrations, J. Clim. 9 (7) (1996) 1518–1530.
[48] H. Van den Dool, A new look at weather forecasting through analogues, Mon. Weather Rev. 117 (10) (1989) 2230–2247.
[49] X. Wang, C.H. Bishop, A comparison of breeding and ensemble transform kalman filter ensemble forecast schemes, J. Atmos. Sci. 60 (9) (2003) 1140–1158.
[50] H.C. Hartmann, T.C. Pagano, S. Sorooshian, R. Bales, Confidence builders: evaluating seasonal climate forecasts from user perspectives, Bull. Am. Meteorol. Soc. 83 (5) (2002) 683–698.
[51] I.T. Jolliffe, D.B. Stephenson, Forecast Verification: a Practitioner's Guide in Atmospheric Science, John Wiley & Sons, 2003.
[52] A.H. Murphy, A new vector partition of the probability score, J. Appl. Meteorol. 12 (4) (1973) 595–600.
[53] [Online; accessed 9-September-2017], Vestas V 90, 2017, https://en.wind-turbine-models.com.
[54] A. Kusiak, H. Zheng, Z. Song, On-line monitoring of power curves, Renew. Energy 34 (6) (2009) 1487–1493.
[55] M. Lydia, A.I. Selvakumar, S.S. Kumar, G.E.P. Kumar, Advanced algorithms for wind turbine power curve modeling, IEEE Trans. Sustain. Energy 4 (3) (2013) 827–835.
[56] M. Lydia, S.S. Kumar, A.I. Selvakumar, G.E.P. Kumar, A comprehensive review on wind turbine power curve modeling techniques, Renew. Sustain. Energy Rev. 30 (2014) 452–460.
[57] M. Hand, S. Baldwin, E. Demeo, J. Reilly, T. Mai, D. Arent, G. Porro, M. Meshek, D. Sandor, Renewable electricity futures study. volume 1. Exploration of high-penetration renewable electricity futures, Tech. rep, National Renewable Energy Lab.(NREL), Golden, CO (United States), 2012.
[58] C. Amante, B.W. Eakins, ETOPO1 1 Arc-Minute Global Relief Model: Procedures, Data Sources and Analysis, U.S. Department of Commerce, National Oceanic and Atmospheric Administration, National Environmental Satellite, Data, and Information Service, National Geophysical Data Center, Marine Geology and Geophysics Division Colorado, 2009.
[59] C. Homer, J. Dewitz, L. Yang, S. Jin, P. Danielson, G. Xian, J. Coulston, N. Herold, J. Wickham, K. Megown, Completion of the 2011 national land cover database for the conterminous United States–representing a decade of land cover change information, Photogramm. Eng. Rem. Sens. 81 (5) (2015) 345–354.
[60] E. Fertig, J. Apt, P. Jaramillo, W. Katzenstein, The effect of long-distance interconnection on wind power variability, Environ. Res. Lett. 7 (3) (2012), 034017.
[61] W. Katzenstein, E. Fertig, J. Apt, The variability of interconnected wind plants, Energy Policy 38 (8) (2010) 4400–4410.
[62] F. Roques, C. Hiroux, M. Saguan, Optimal wind power deployment in Europe: a portfolio approach, Energy Policy 38 (7) (2010) 3245–3256.